

Neutron-Diffraction Measurements of Magnetic Order and a Structural Transition in the Parent BaFe_2As_2 Compound of FeAs-Based High-Temperature Superconductors

Q. Huang,¹ Y. Qiu,^{1,2} Wei Bao,^{3,*} M. A. Green,^{1,2} J. W. Lynn,¹ Y. C. Gasparovic,^{1,2} T. Wu,⁴ G. Wu,⁴ and X. H. Chen⁴

¹*NIST Center for Neutron Research, National Institute of Standards and Technology, Gaithersburg, Maryland 20899, USA*

²*Department of Materials Science and Engineering, University of Maryland, College Park, Maryland 20742, USA*

³*Los Alamos National Laboratory, Los Alamos, New Mexico 87545, USA*

⁴*Hefei National Laboratory for Physical Science at Microscale and Department of Physics, University of Science and Technology of China, Hefei, Anhui 230026, China*

(Received 14 July 2008; published 17 December 2008)

The recent discovery of superconductivity in $(\text{Ba}, \text{K})\text{Fe}_2\text{As}_2$, which crystallizes in the ThCr_2Si_2 (122) structure as compared with the LnFeAsO (Ln is lanthanide) systems that possess the ZrCuSiAs (1111) structure, demonstrates the exciting potential of the FeAs-based materials for high- T_C superconductivity. Here we report neutron diffraction studies that show a tetragonal-to-orthorhombic distortion associated with the onset of $\mathbf{q} = (101)$ antiferromagnetic order in BaFe_2As_2 , with a saturation moment $0.87(3)\mu_B$ per Fe that is orientated along the longer a axis of the ab planes. The simultaneous first-order structural and magnetic transition is in contrast with the separated transitions previously reported in the 1111-type materials. The orientational relation between magnetic alignment and lattice distortion supports a multiorbital nature for the magnetic order.

DOI: 10.1103/PhysRevLett.101.257003

PACS numbers: 74.25.Ha, 61.05.fm, 74.70.-b, 75.30.Fv

In addition to high superconducting transition temperatures ($T_C \approx 55$ K) [1–4], the newly discovered iron oxypnictide superconductors offer additional compositional variation. The family of FeAs-based superconductors with the same 1111-type structure now include LnFeAs (O,F), Ln = La, Sm, Ce, Nd, Pr, Gd, Tb, or Dy [1–12]. In a similar fashion to the CuO_2 layers present in cuprates, the FeAs layers have been shown in theory to dominate the electronic states at the Fermi level that produce superconductivity [13–15]. Cuprate superconductors distinguish themselves structurally by adopting different stacking sequences of the CuO_2 and electronically inactive “spacer” layers. Using the same structural philosophy, layered materials with the formula $(\text{A}, \text{K})\text{Fe}_2\text{As}_2$, A = Ba or Sr, which crystallize in a different 122-type structure, have recently been reported and possess a T_C as high as 38 K [16–19].

Like the parent compounds LnFeAsO of the 1111-type FeAs superconductors, the 122-type parent compounds BaFe_2As_2 and SrFe_2As_2 are not superconducting and show a similar pronounced anomaly in resistivity at $T_S \sim 140$ K [16,19,20] and 205 K [17,18,21], respectively. Structural refinements have been performed only for BaFe_2As_2 using x-ray powder diffraction, and a second-order structural phase transition like in LaFeAsO at T_S has been concluded, which also cause an anomaly in susceptibility [20]. The ^{57}Fe Mössbauer spectra have been measured at 298, 77, and 4.2 K for BaFe_2As_2 , and long-range magnetic order exists at 77 and 4.2 K [20]. No such spectroscopic studies have yet been performed for SrFe_2As_2 . Careful specific heat measurements, however, indicate the phase transition at $T_S \approx 205$ K in SrFe_2As_2 as a first-order one [21]. So far, no magnetic structure in the

new 122-type materials has been reported, neither is it clear whether the magnetic transition concurs with the structural transition at T_S or is a separate phase transition as in LaFeAsO [22,23] or NdFeAsO [24].

Here, we report neutron diffraction studies of BaFe_2As_2 that completely determine its magnetic structure. The antiferromagnetic alignment and magnetic moment are both along the longer a axis in the FeAs plane, which could not be determined previously in LaFeAsO [22]. The structural transition is shown to be first order by thermal hysteresis in the splitting of the Bragg peak. In contrast to the separate second-order structural and magnetic transitions reported previously for the 1111-type materials [22,23], the magnetic transition occurs at the same temperature where the structural transition from tetragonal to orthorhombic symmetry also occurs. Although the magnetic and structural transitions occur differently in the BaFe_2As_2 and the 1111-type materials, this work clearly demonstrates that the complete evolution to a low symmetry structure is a prerequisite for the common iron magnetic order to occur.

We synthesized 2 g of polycrystalline BaFe_2As_2 sample using the solid state reaction as described in Ref. [19]. The resistivity was measured using the standard four-probe method while the sample was cooled. As shown in Fig. 1, the drop of resistivity at $T_S \sim 142$ K is sudden and steep, as previously reported [20,21]. Neutron powder diffraction spectra were measured with neutrons of wavelength $\lambda = 2.079$ Å, using the high resolution powder diffractometer BT1 at the NIST Center for Neutron Research (NCNR). The sample temperature was controlled by a closed cycle refrigerator. The spectrum measured at 175 K is shown in Fig. 2(a) together with the refined profile

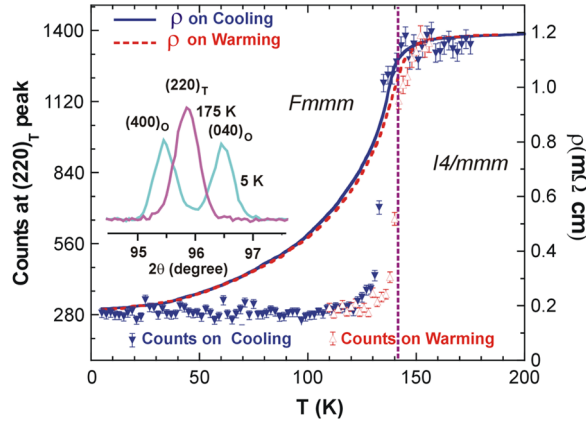


FIG. 1 (color online). The resistivity of BaFe_2As_2 as a function of temperature, measured while cooling then warming, shows a sharp drop at $T_S \sim 142$ K. The resistivity anomaly is associated with a first-order structural transition, as indicated by the hysteresis in neutron diffraction intensity at diffraction angle $2\theta = 95.8^\circ$. Inset: Neutron diffraction spectra measured above and below the structural transition, showing the splitting of the peak below T_S .

obtained with the GSAS program [25]. Consistent with previous studies [20], the high-temperature structure is well accounted for by the tetragonal ThCr_2Si_2 -type structure, and the structural parameters from the refinement using space group $I4/mmm$ are listed in Table I(a).

The neutron powder diffraction spectrum measured at 5 K is shown in Fig. 2(b). Our neutron data confirm the orthorhombic structural distortion previously reported in the x-ray study [20], which splits the $(220)_T$ Bragg peak of the $I4/mmm$ tetragonal unit cell, shown in the inset of Fig. 2(a), into two Bragg peaks $(400)_O$ and $(040)_O$ of the $Fmmm$ orthorhombic unit cell as marked in Fig. 2(b). To clarify the nature of the structural transition at $T_S \sim 142$ K, we followed the diffraction intensity at $2\theta = 95.8^\circ$ as a function of temperature. Above T_S , this angle corresponds to the peak position of the $(220)_T$; below T_S , it corresponds

TABLE I. Structure and magnetic parameters of BaFe_2As_2 . (a) At 175 K, $I4/mmm$ (No. 139): $a = b = 3.95702(4)$, $c = 12.9685(2)$ Å. $R_p = 4.71\%$, $wRp = 6.06\%$, $\chi^2 = 1.109$. (b) At 5 K, $Fmmm$ (No. 69): $a = 5.61587(5)$, $b = 5.57125(5)$, $c = 12.9428(1)$ Å. $R_p = 3.61\%$, $wRp = 4.58\%$, $\chi^2 = 1.825$.

(a)	Site	x	y	z	B (Å ²)	
Ba	$2a$	0	0	0	0.53(5)	
Fe	$4d$	1/2	0	1/4	0.72(2)	
As	$4e$	0	0	0.35405(8)	0.80(3)	
(b)	Site	x	y	z	B (Å ²)	M_x (μ _B)
Ba	$4a$	0	0	0	0.20(4)	
Fe	$8f$	1/4	1/4	1/4	0.35(2)	0.87(3)
As	$8i$	0	0	0.35406(7)	0.47(3)	

to the valley between the $(400)_O$ and $(040)_O$ peaks; see inset of Fig. 1. The intensity changes in a steplike first-order fashion as shown in Fig. 1. Additionally, hysteresis was observed during a cooling and warming cycle with a temperature change rate of 15 K per hour. Therefore, while the pronounced anomaly in resistivity is associated with the tetragonal-to-orthorhombic structural transition in both the 122 and 1111 types of the FeAs-based materials, the structural transition in the newer 122-type material occurs in a first-order transition.

Additional magnetic Bragg peaks are apparent in the neutron diffraction patterns measured below T_S . Analysis of the magnetic Bragg reflections reveals a simple antiferromagnetic structure within the eight Fe ions in the orthorhombic unit cell. The fundamental magnetic wave vector is $\mathbf{q} = (101)_O$. In the inset of Fig. 2(b), magnetic Bragg peaks from the 5 K spectrum are highlighted by the vertical lines and are indexed using the orthorhombic unit cell. The in-plane magnetic moment has a twofold symmetry [26]; namely, it is either along the a or b axis of the $Fmmm$ unit cell. Refinement yields that the magnetic mo-

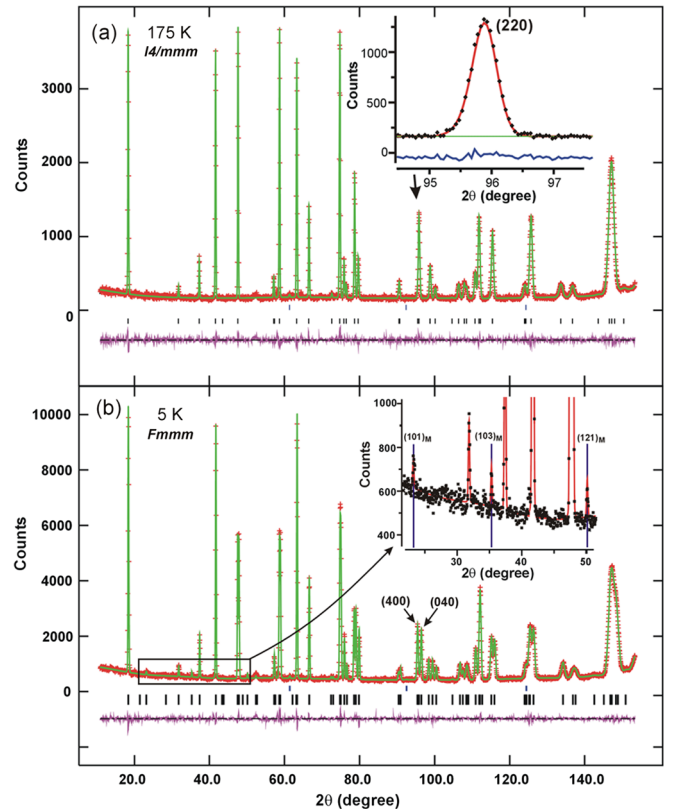


FIG. 2 (color online). Neutron powder diffraction spectra at (a) 175 and (b) 5 K. The high-temperature spectrum is refined with the tetragonal $I4/mmm$ space group; the low temperature one with the orthorhombic $Fmmm$ space group together with the magnetic structure shown in Fig. 3. The (220) Bragg peak in (a) is split into the (400) and (040) in (b) by the orthorhombic structural distortion. Magnetic peaks at 5 K are highlighted in the inset of (b).

ment is parallel to the a axis. The magnetic and crystal parameters determined in a combined structural and magnetic refinement of the 5 K spectrum are listed in Table I(b), and the magnetic structure of BaFe_2As_2 is depicted in the bottom row of Fig. 3.

It should be noted that the Fe antiferromagnetic order occurs in the orthorhombic crystal structure below T_S , and the a and b axes are not equivalent. For LaFeAsO , although the magnetic structure is depicted along one axis, that was a representational solution, and both the moment direction and the antiferromagnetic wave vector direction in the FeAs plane were not determined due to weaker magnetic intensity [22]. For BaFe_2As_2 , our powder neutron data unequivocally determine the ferromagnetic row of Fe magnetic moments as along the shorter b axis, and these rows of Fe moments align antiferromagnetically along the longer a axis in the FeAs plane (see the bottom row of Fig. 3). For comparison, the choice of (011) as the magnetic wave vector would not be consistent with the measured spectrum as shown in the upper row of Fig. 3.

For magnetic order originating from a single orbital, the odd symmetry between the neighboring pair of orbitals of parallel spins, demanded by the Pauli principle, expands the neighbor distance. Likewise, the distance between antiparallel spins contracts due to the even orbital symmetry. This is opposite to what we observed in BaFe_2As_2 . Our observed magnetostriction can be understood when magnetism is contributed from multiple d orbitals, and is consistent with conclusion from a previous first-principle

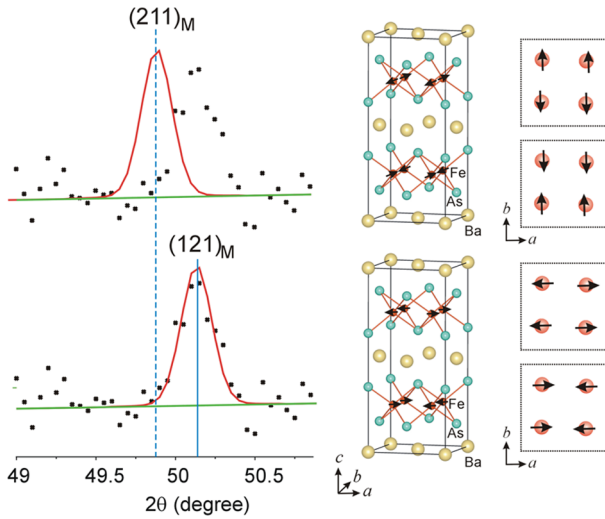


FIG. 3 (color online). Magnetic and crystal structures of BaFe_2As_2 . The magnetic Bragg profiles of two magnetic models are shown in two rows, respectively. The moment orientation in the two Fe layers of the orthorhombic $Fmmm$ unit cell is highlighted on the side. The measured magnetic Bragg peak is well represented by the (121) index (bottom), not the (211) (top). Therefore, the magnetic wave vector is (101); namely, the Fe magnetic moments are aligned antiferromagnetically along the a and c axes, and ferromagnetically along the b axis (bottom).

calculations for LaFeAsO [27] which shares with BaFe_2As_2 the same electronically active FeAs layers.

Although the directions of \mathbf{q} and moment have not been determined in the orthorhombic phase of LaFeAsO [22], the magnetic structure of BaFe_2As_2 has the identical relative phase relation among the Fe moments to that of LaFeAsO . This demonstrates a commonality of the magnetic interactions within the Fe layers. Variation in the stacking of the layers, and therefore variation in the interactions along the c axis, does not alter the overall magnetic structure.

The ordered magnetic moment $0.87(3)\mu_B$ per Fe at 5 K in BaFe_2As_2 is substantially larger than the saturated moment $0.36(5)\mu_B$ per Fe in LaFeAsO [22], but is comparable to the iron moment $0.9(1)\mu_B$ in a different combined Fe and Nd antiferromagnetic structure in NdFeAsO [24]. BaFe_2As_2 differs most significantly from LaFeAsO in that the antiferromagnetic transition occurs at a temperature that is indistinguishable from the structural transition, in contrast to all previously measured FeAs-based 1111-type materials where structural and magnetic transitions are separate ones [22–24]. Figure 4 shows the temperature dependence of the magnetic Bragg peak $(101)_M$, measured at the higher flux triple-axis spectrometer BT7 at NCNR while the sample temperature was raised. The solid line represents the mean-field theoretical fit for the squared magnetic order parameter, and the Néel temperature is determined at $T_N \approx 143(4)$ K, which is the same value determined for the structural transition. It is clear from these measurements that the important criterion for the onset of magnetic order is the complete disappearance of the high-temperature phase.

Soon after the discovery of the LaFeAs(O,F) superconductor [5], it was recognized that there exist nesting Fermi surfaces connected by the wave vector $(1/2, 1/2, 0)_T$ in the calculated electronic band structures of the parent compound LaFeAsO [28–30], and the resistivity anomaly of

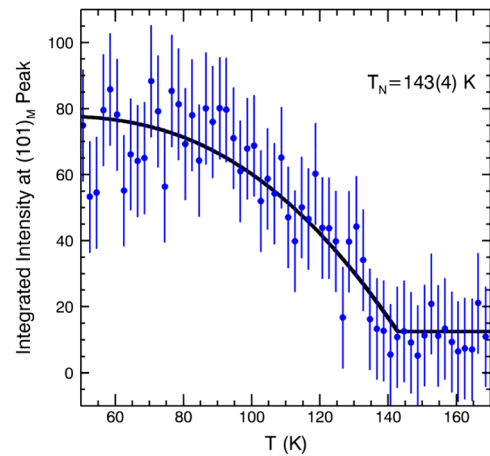


FIG. 4 (color online). Magnetic Bragg peak $(101)_M$ as a function of temperature. The solid line represents the least-squares fit to mean-field theory for the squared order parameter.

LaFeAsO at ~ 150 K was predicted to be caused by the resulting spin-density-wave (SDW) order [31]. Since the electronic states near the Fermi surfaces come predominantly from the five d orbitals of the Fe ions [13–15], the SDW represents an antiferromagnetic order of Fe. The antiferromagnetic spin fluctuations characterized by the SDW wave vector $(1/2, 1/2, 0)_T$ have been invoked in a large number of theoretical works as the bosonic mode to mediate the Cooper pair formation in the FeAs-based new high- T_C superconductors. It turns out that the anomaly is instead associated with a structural transition, and the antiferromagnetic transition was observed at ~ 137 K in a separated phase transition [22]. Additionally, the observed magnetic moment of the Fe ion is an order of magnitude weaker than the theoretically predicated $\sim 2.3\mu_B$ per Fe [29,30]. Frustrating magnetic exchange interactions have to be invoked to explain the small observed moment in LaFeAsO [27,32]. In another 1111-type material, NdFeAsO, for which magnetic structure has been determined, substantially larger moment $0.9\mu_B/\text{Fe}$ was observed below 1.96 K in a combined Nd and Fe antiferromagnetic order, while the resistivity anomaly and the structural transition concur at ~ 140 K [24].

While the predication of the resistivity anomaly caused by the SDW transition has not been realized for the intended 1111-type materials, it is interesting that it occurs in BaFe₂As₂ in the structurally simpler 122-type materials. The concurring first-order structural and magnetic transition indicates strong coupling between the structural and magnetic order parameters. A similar previous experimental observation has led to the identification of an orbital ordering among degenerate d orbitals as the driving force of a first-order structural transition in the vicinity of a SDW transition [33]. There are degenerate Fermi sheets from the Fe d orbitals for the FeAs-based materials in the tetragonal phase [28–30]. The structural transition could in principle break the degeneracy and involve the orbital degree of freedom in the combined magnetic and structural transition.

In summary, a consistent picture covering both the 1111- and 122-type materials is that the Fe magnetic order in the common FeAs layer is the same with the magnetic wave vector $(1/2, 1/2, 0)_T$, which conforms to the orthorhombic symmetry. The occurrence of the Fe magnetic order is contingent upon the orthorhombic structural distortion. In BaFe₂As₂, the orthorhombic distortion is consistent with magnetostriction expected for magnetism from multiple d orbitals [27]. The pronounced anomaly in resistivity is associated with the concurring structural and magnetic transition. Like the CuO₂ layers in various cuprates, the FeAs layers have been shown to control similar physical processes in both 122- and 1111-type materials.

Work at LANL is supported by U.S. DOE-OS-BES; at USTC by the Natural Science Foundation of China,

Ministry of Science and Technology of China (973 Project No. 2006CB601001), and by National Basic Research Program of China (2006CB922005).

Note added.—Su *et al.* [34] reported a magnetic wave vector along the shorter axis of the ab plane, a magnetic transition at 100 K, and decoupled magnetic and structural transitions in a neutron diffraction work using BaFe₂As₂ single crystals grown from Sn flux, in sharp contrast to our results which are consistent with our later measurements using BaFe₂As₂ single crystals grown by a self-flux method. It is known that the Sn flux-grown BaFe₂As₂ single crystals have serious sample-quality issue [26].

*wbao@lanl.gov

- [1] Z. A. Ren *et al.*, Chin. Phys. Lett. **25**, 2215 (2008).
- [2] R. H. Liu *et al.*, Phys. Rev. Lett. **101**, 087001 (2008).
- [3] Z.-A. Ren *et al.*, Europhys. Lett. **83**, 17 002 (2008).
- [4] C. Wang *et al.*, Europhys. Lett. **83**, 67 006 (2008).
- [5] Y. Kamihara *et al.*, J. Am. Chem. Soc. **130**, 3296 (2008).
- [6] X. H. Chen *et al.*, Nature (London) **453**, 761 (2008).
- [7] G. F. Chen *et al.*, Phys. Rev. Lett. **100**, 247002 (2008).
- [8] Z. A. Ren *et al.*, Europhys. Lett. **82**, 57 002 (2008).
- [9] Z. A. Ren *et al.*, Mater. Res. Innovations **12**, 105 (2008).
- [10] G. F. Chen *et al.*, Chin. Phys. Lett. **25**, 2235 (2008).
- [11] Z. A. Ren *et al.*, Supercond. Sci. Technol. **21**, 082001 (2008).
- [12] J.-W. G. Bos *et al.*, Chem. Commun. (Cambridge) **31**, 3634 (2008).
- [13] D. J. Singh and M.-H. Du, Phys. Rev. Lett. **100**, 237003 (2008).
- [14] K. Haule *et al.*, Phys. Rev. Lett. **100**, 226402 (2008).
- [15] G. Xu *et al.*, Europhys. Lett. **82**, 67 002 (2008).
- [16] M. Rotter *et al.*, Phys. Rev. Lett. **101**, 107006 (2008).
- [17] G. F. Chen *et al.*, Chin. Phys. Lett. **25**, 3403 (2008).
- [18] K. Sasmal *et al.*, Phys. Rev. Lett. **101**, 107007 (2008).
- [19] G. Wu *et al.*, Europhys. Lett. **84**, 27 010 (2008).
- [20] M. Rotter *et al.*, Phys. Rev. B **78**, 020503(R) (2008).
- [21] C. Krellner *et al.*, Phys. Rev. B **78**, 100504 (2008).
- [22] C. de la Cruz *et al.*, Nature (London) **453**, 899 (2008).
- [23] T. Nomura *et al.*, Supercond. Sci. Technol. **21**, 125028 (2008).
- [24] Y. Qiu *et al.*, preceding Letter, Phys. Rev. Lett. **101**, 257002 (2008).
- [25] A. Larson and R. B. Von Dreele, GSAS: Generalized Structure Analysis System (1994).
- [26] X. F. Wang *et al.*, arXiv:0806.2452.
- [27] T. Yildirim, Phys. Rev. Lett. **101**, 057010 (2008).
- [28] I. I. Mazin *et al.*, Phys. Rev. Lett. **101**, 057003 (2008).
- [29] C. Cao *et al.*, Phys. Rev. B **77**, 220506 (2008).
- [30] F. Ma and Z. Y. Lu, Phys. Rev. B **78**, 033111 (2008).
- [31] J. Dong *et al.*, Europhys. Lett. **83**, 27 006 (2008).
- [32] Q. Si and E. Abrahams, Phys. Rev. Lett. **101**, 076401 (2008).
- [33] W. Bao *et al.*, Phys. Rev. Lett. **78**, 507 (1997).
- [34] Y. Su *et al.*, arXiv:0807.1743.